Science Translational Medicine
AAAS

www.sciencetranslationalmedicine.org/cgi/content/full/9/381/eaaf2968/DC1

Supplementary Materials for

Disrupting the CD47-SIRPα anti-phagocytic axis by a humanized anti-CD47 antibody is an efficacious treatment for malignant pediatric brain tumors

Sharareh Gholamin, Siddhartha S. Mitra,* Abdullah H. Feroze, Jie Liu, Suzana A. Kahn, Michael Zhang, Rogelio Esparza, Chase Richard, Vijay Ramaswamy, Marc Remke, Anne K. Volkmer, Stephen Willingham, Anitha Ponnuswami, Aaron McCarty, Patricia Lovelace, Theresa A. Storm, Simone Schubert, Gregor Hutter, Cyndhavi Narayanan, Pauline Chu, Eric H. Raabe, Griffith Harsh IV, Michael D. Taylor, Michelle Monje, Yoon-Jae Cho, Ravi Majeti, Jens P. Volkmer, Paul G. Fisher, Gerald Grant, Gary K. Steinberg, Hannes Vogel, Michael Edwards, Irving L. Weissman, Samuel H. Cheshier*

*Corresponding author: Email: ssmitra@stanford.edu (S.S.M.); cheshier@stanford.edu (S.H.C.)

Published 15 March 2017, *Sci. Transl. Med.* **9**, eaaf2968 (2017)
DOI: 10.1126/scitranslmed.aaf2968

The PDF file includes:

Other Supplementary Material for this manuscript includes the following:
(available at
www.sciencetranslationalmedicine.org/cgi/content/full/9/381/eaaf2968/DC1)

Movie S1 (.mov format). Qualitative behavioral assessment of SU_MB002 tumor-bearing mice treated with Hu5F9-G4 compared to control.
Movie S2 (.mov format). Qualitative behavioral assessment of D425s tumor-bearing mice treated with Hu5F9-G4 compared to control.

Materials and Methods

Description of therapeutic antibody used (Hu5F9-G4). Hu5F9-G4 was constructed using CDR-grafting from a mouse anti-human CD47 antibody, clone 5F9. Because Hu5F9-G4 activity is primarily dependent on blocking the CD47-SIRP α interaction, a human IgG4 scaffold was selected to minimize the recruitment of Fc-dependent effector functions such as antibody-dependent cellular cytotoxicity, antibody-dependent cellular phagocytosis, and complement-dependent cytotoxicity. The mechanism of action does not require these functions, and their presence may increase toxicity against normal cells. Hu5F9-G4 was engineered using a human kappa and IgG4 isotype with a Ser228Pro substitution to reduce Fab arm exchange. Detailed biochemical characterization and non-human primate safety assessment was previously published (*22*).

Primary tissue dissociation and generation of primary cell lines. Pediatric brain tumor tissue samples were obtained under IRB protocol ID 18672 after informed patient consent at the Lucile Packard Children's Hospital (Stanford, CA) in accordance with institutional review board protocols. For minors, consent was obtained from a parent or guardian. Human subjects approval was given under IRB number: 350 (Panel: 3). Tumor pathology and diagnosis were confirmed by the on call institutional neuropathologist. Samples were enzymatically dissociated to single cells by collagenase IV (1 mg/ml) and DNase I (250 units/ml), and cells were plated in neural stem cell expansion medium (NSCEM) consisting of Neurobasal (-A) (Invitrogen), B27 (-A) (Invitrogen), human-bFGF (20 ng/ml) (Shenandoah Biotech), human-EGF (20 ng/ml) (Shenandoah Biotech), human recombinant LIF (Millipore) (as required), and heparin (10 ng/ml)(*28*). Pediatric glioblastoma cells were plated in pediatric glioma stem cell expansion medium (GSCEM) consisting of Neurobasal (-A) (Invitrogen), B27 (-A) (Invitrogen), human-

bFGF (20 ng/ml) (Shenandoah Biotech), human-EGF (20 ng/ml) (Shenandoah Biotech), human PDGF-AA (20 ng/ml), PDGF-BB (20 ng/ml) (Shenandoah Biotech), and heparin sulfate (10 ng/ml) (Sigma). Cells were grown for 2 passages and infected with EF1-GFP-T2A-Luciferase (Systems Biosciences, BLIV503MN-1), then allowed to re-form spheres. Cells were then double sorted for GFP and further passaged in neural stem cell medium. Human fetal brain tissue from gestational weeks 16 to 22 was obtained from a non-profit source (Stem Express) and dissociated to single cells using TryPLE (Life Technologies), then cultured in NSCEM, as described above.

Primary human pediatric brain tumor cell lines. The primary cell lines were generated at Stanford University in our laboratory or kindly provided by various collaborators as detailed below. All tumor lines were authenticated using short tandem repeat (STR) fingerprinting at the following 15 loci: D3S1358, TH01, D21S11, D18S51, Penta E, D5S818, D13S317, D7S820, D16S539, CSF1PO, Penta D, vWA, D8S1179, TPOX, FGA, AMEL. All cultures were routinely tested for mycoplasma contamination.

Pediatric glioma lines. SU_DIPGVI, SU_DIPGXIII, and JHH DIPG1 (*56*) were from rapid autopsy specimens of patients who died from diffuse intrinsic pontine glioma after receiving radiation and chemotherapy. SU_pGBM001 and SU_pGBM002 were derived from surgically resected tumor samples of pediatric patients diagnosed with glioblastoma.

Atypical teratoid rhabdoid tumor lines. CHB-ATRT1 was derived from a surgical specimen of a tumor from the posterior fossa. SU_ATRT002 was derived from a supratentorial surgical specimen.

MB lines. D283 and D425 were generously provided by Dr. Darrell Bigner (Duke University, Durham, NC). D425s was subcloned from the original D425 for increased growth characteristics and incidence of spinal metastasis. SU_MB002 cells were derived postmortem from the

leptomeningeal compartment of a child with metastatic, treatment-refractory (chemotherapy only) MB. SU_MB009 cells were derived from the primary surgical resection of a tumor in a child whose tumor recurred after therapy, and they have been described earlier (*57*). SU_MB012 and SU_MB014 were derived from the primary surgical resection of a tumor in a child whose tumor recurred after therapy. MYC amplification in the SU_MB002 and D425s cells was confirmed with NanoString nCounter v2 Cancer CN Codeset.

Human neural progenitor lines: Origin and maintenance. Neural progenitor line (NSC1) was derived from subventricular zone tissue surgically excised during a functional hemispherectomy in a child with refractory seizures. NSC2 was derived from human fetal brain tissue from gestational weeks 16 to 22. Human neural progenitor cell lines were routinely tested for multi-potency and neurosphere self-renewal using standard protocols (*28*).

GL261 mouse glioma cell line. GL261 was a kind gift from Dr. Michael Lim (Johns Hopkins University). The GL261 murine glioma model was established in 1970 by chemical induction with methylcholanthrene. Tumors generated were serially transplanted subcutaneously and intracranially in C57BL/6 mice. The list of primary cell lines used in this study is shown in table S2.

Cell line maintenance. Primary pGBM and DIPG lines were maintained in serum-free glioma stem cell medium consisting of Neurobasal (-A) (Invitrogen), B27 (-A) (Invitrogen), human-bFGF (20 ng/ml) (Shenandoah Biotech), human-EGF (20 ng/ml) (Shenandoah Biotech), human PDGF-AA (20 ng/ml), PDGF-BB (20 ng/ml) (Shenandoah Biotech), and heparin sulfate (10 ng/ml). All patient-derived MB primary cells were maintained in NSCEM. The subventricular zone-derived neural stem cells were similarly maintained in NSCEM. All patient-derived cell lines were authenticated using sequence-tagged site fingerprinting. Each line was evaluated for

its ability to fully recapitulate the tumor of origin by orthotopic transplantation into NSG mice and analysis of the engrafted tumors by H&E staining.

Orthotopic transplantation of brain tumors and neural progenitor cells. Early passage spheres were transduced with either GFP or Td-tomato and luciferase-encoding lentivirus, expanded in (GSCEM), and double sorted for GFP or Td-tomato expression to obtain a >95% luciferase-expressing population. The selected population was expanded in (GSCEM) and orthotopically injected into the site of tumor resection. pHGG and ATRT cells were injected 2 mm posterior to bregma, 2 mm lateral to midline, and 3-4 mm deep in the brain. MB, PNET, and DIPG cells were injected at coordinates 2 mm posterior to lambda on midline and 2 mm deep into 4-6-week-old NOD-SCIDγ mice. Fetal brain-derived NPCs were injected in the lateral hemisphere of 1 to 3-day-old pups.

Flow cytometry analysis. Surgical brain tumor specimens were dissociated to single cells and stained with anti-CD47-PE. Hematopoietic and endothelial cells were gated out using a lineage mixture of Pacific blue conjugated anti-CD45 and anti-CD31. For analysis of MB initiating cells in xenografts, tumor-bearing mouse brains were dissociated to single cells. Anti-H2kb and anti-H2kd (Biolegend) antibodies were used to gate out mouse cells, and anti-CD15-FITC (BD Biosciences: Clone MMA) mAb was used to identify CD15+ human MB initiating cells. Flow cytometric analysis and cell sorting were performed on the BD FACS aria II (Becton Dickinson). Appropriate isotype and fluorescence, minus one control, were used to define the background gates.

Osmotic pump implantation. To achieve continuous intraventricular CNS administration of the anti-CD47 antibody, osmotic pumps (Alzet Co., Model 1004; flow rate 0.11 µL/h) were loaded with 1.9 µg/µL of antibody (equivalent to previously established 10 mg/kg dosing) or phosphate-

buffered saline (PBS) (control). Pumps were coupled to brain infusion kits (Alzet Co., Model 8851) and primed overnight at 37 °C, 5% CO2. Osmotic pumps were implanted subcutaneously on the dorsum, slightly caudal to the scapulae, through a 2.5 cm midline incision. Using a stereotaxic apparatus, brain cannulae were inserted intraventricularly per predefined coordinates (2 mm posterior to bregma, 0.5 mm right of midline, 1 mm deep) after removal of periosteal connective tissue, and secured with dental cement (Stoelting Co.). At the time of animals' death, cannula patency and drug delivery were verified by comparing pump weight before and after implantation.

In vivo sequential co-transplant xenograft cytotoxicity model. Human fetal-derived neural progenitor cells expressing Td-tomato and luciferase were injected into the lateral ventricle, 0.5 mm lateral to midline, of neonatal NSG mouse pups at 1 to 3 days of age. Mice were followed with BLI to ensure engraftment and sustained expression of luciferase. Human progenitor engrafted mice were then injected with unlabeled human MB cells (SU_MB002) at 1.5 months of age. SU_MB002 was previously confirmed (*58*) to have 100% penetrance in multiple cohorts. 14 d after tumor cell transplantation, the mice were randomized based on BLI values and treated with either Hu5F9-G4 or PBS. Human neural cell viability and proliferation were measured through subsequent BLI.

Immunohistochemistry. Expression of CD47 protein on primary tumor samples was evaluated on 4-μm thick OCT embedded fresh frozen tissue sections. Sections were fixed with acetone, blocked with 5% goat serum, and incubated with anti-CD47 antibody (0.2 μg/ml, Abcam ab3283) followed by goat anti-mouse Alexa488 (Invitrogen) secondary antibody and counter-stained with 4',6-diamidino-2-phenylindole (DAPI). The sections were mounted, and the imaging was done on a fluorescent microscope (Leica). Orthotopic tumor-bearing mouse brains were

fixed in formalin and embedded in paraffin, and 8 μm sections were cut to reveal either coronal or sagittal views of the brains. Tissue sections were processed for standard H&E staining or for mouse macrophage markers using the anti-F4/80 (Abcam) antibody. The images were taken with a Nikon E1000M microscope with a Spot Flex camera.

In vitro phagocytosis assay. In vitro phagocytosis assay was performed as described before (*10*) with both human and mouse macrophages analyzed by either FACS or microscopy. To obtain human monocytes, PBMCs collected from venous blood of healthy volunteers were separated on a Ficoll density gradient (GE Healthcare). CD14+ monocytes were positively selected to >95% purity by MACS using anti-CD14 microbeads (Miltenyi), then plated at 1 x 10^6/ml in 150 x 25 mm tissue culture plates in RPMI 1640 with 10% FBS, penicillin/streptomycin, glutamine, and HEPES. To generate monocyte-derived macrophages, monocytes were treated for 7 d with human recombinant M-CSF (25 ng/mL). Mouse macrophages were obtained from mouse bone marrow after 7 d of bone marrow cell plating with mouse colony stimulating factor.

For phagocytosis assays carried out by fluorescence microscopy, macrophages were stained with PKH26 (Sigma-Aldrich), and dissociated tumor cells were labeled with 2.5 μM carboxyfluorescein succinimidyl ester (CSFE) according to the manufacturer's description. Cells were co-incubated at a 1:2 ratio (macrophages:tumor cells) along with indicated antibodies (10 μg/ml) or human IgG controls and incubated for 2 h at 37 °C. Wells were repeatedly washed to remove non-phagocytosed cells and subsequently imaged with an inverted microscope (Leica DMI6000B). The phagocytic index was calculated as the number of macrophages that had phagocytosed tumor cells per 100 macrophages. For FACS-based phagocytosis assay, CFSE labeled tumor cells were incubated with indicated antibodies (10 μg/ml) for 30 min at 37 °C before co-incubation with macrophages. Adherent macrophages were collected using TrypLE

Express (Life Technologies) and incubated in serum-free medium. 5 x 10^4 macrophages were added to 1 x 10^5 CFSE-labeled live tumor cells per well for 4 h and returned to the incubator. Analysis was carried out by flow cytometry. Human macrophages were identified using anti-human CD11b-Alexa647 and anti-human CD14- APC/Cy7 (BioLegend). Phagocytosis assays for each tumor type were performed in triplicates and repeated at least two times.

Sorting of macrophage populations during phagocytosis. Macrophages (count 500,000) were incubated with MB cells (2 million) labeled with Calcein-AM (Life Technologies) in the presence of Hu5F9-G4 for 2 h. The population that was positive for macrophages (identified using anti-CD14 and anti-CD11b antibodies) and MB cells (identified with Calcein) was sorted, cytospun onto slides, stained with modified Wright-Giemsa Stain (Sigma-Aldrich) according to the manufacturer's instructions, and imaged with light microscopy.

Collection of cerebrospinal fluid. CSF sampling was performed from the cisterna magna, located between the cerebellum and dorsal surface of the spinal cord. The mouse was shaved in the neck area, anesthetized with isoflurane, and placed in a stereotaxic frame. A midline sagittal incision was made inferior to the occiput. The pyramid muscles were separated using blunt forceps. To get proper access to dura mater of the cisterna magna, the mouse head was repositioned making a 135-degree angle with the body. Subsequently, the dura mater of cisterna magna was punctured using a glass capillary. Five to ten microliters of clean CSF sample was drained from the cisterna magna. Samples testing positive for blood serum albumin or hemoglobin were discarded from analysis.

Enzyme-linked immunosorbent assay (ELISA) for testing Hu5F9-G4 levels in blood and CSF. Ninety-six-well plates (Costar, 9018) were coated with huCD47/mFc at a concentration of 1 μg/ml in PBS and incubated at 4 °C overnight. After the plates were blocked for 1 h with 0.4%

bovine serum albumin in PBS at room temperature, mouse serum and CSF samples were added in four sequential dilutions. The plates were incubated for 1 h at room temperature. Ten micrograms/ml biotin-labeled mouse 5F9 was added to the wells in the presence of various concentrations of unlabeled Hu5F9-G4, and the plates were incubated at room temperature for 1 h. After three successive washing steps, the plates were then incubated with HRP conjugated goat anti-human kappa-specific antibody for 1 h at room temperature. Plates were developed with OPT. The reaction was stopped with 2M H_2SO_4, and the results were recorded as optical density units at 490 nM. GraphPad Prism (GraphPad Inc.) was used to analyze the data.

Mice. NOD.Cg-Prkdcscid Il2rgtm1Wjl/SzJ (NSG) and C57/BL6 mice were housed in specific pathogen-free conditions at a barrier facility at the Lokey Stem Cell Building at Stanford School of Medicine (Stanford, CA). All animal handling, surveillance, and experimentation were performed in accordance with and approval from the Stanford University Administrative Panel on Laboratory Animal Care (Protocol # 26548 and 26209).

Tumor tissue dissociation. Tumor samples were enzymatically dissociated by collagenase IV (1 mg/ml) in dissociation solution containing HBSS with calcium/magnesium (Cellgro), non-essential amino acids (Cellgro), sodium pyruvate (Cellgro), sodium bicarbonate (Cellgro), HEPES (25 mM) (Cellgro), 1X Glutamax-1 (Cellgro), 1X antibiotic antimycotic (Cellgro), DNase, and collagenase IV (Worthington) at 37 °C. The suspension was washed 2 times with HBSS and filtered using 100 μm and 40 μm filters, respectively. The cells were resuspended in 0.9 M sucrose gradient solution in HBSS without Ca/Mg (Cellgro) to remove debris and dead cells. The cells were treated with ACK/RBC lysis buffer (Gibco), washed twice in PBS, and were then ready to use. For neurosphere formation, single tumor cells were plated in tumor-stem medium (TSM) consisting of Neurobasal (-A) (Invitrogen), B27 (-A) (Invitrogen), human-bFGF

(20 ng/ml) (Shenandoah Biotech), human-EGF (20 ng/ml) (Shenandoah Biotech), human recombinant LIF (Millipore), and heparin (10 ng/ml). Early passage spheres were transduced with either GFP or Td-tomato luciferase encoding lentivirus and expanded in TSM. After secondary tumor sphere formation, the GFP or Td-tomato-positive cells were double sorted to obtain a pure population. The selected population was expanded in TSM medium and then injected intracranially into 5-6-week-old NSG mice using the stereotaxic frame.

Supplementary Figures

Supplementary Figure 1

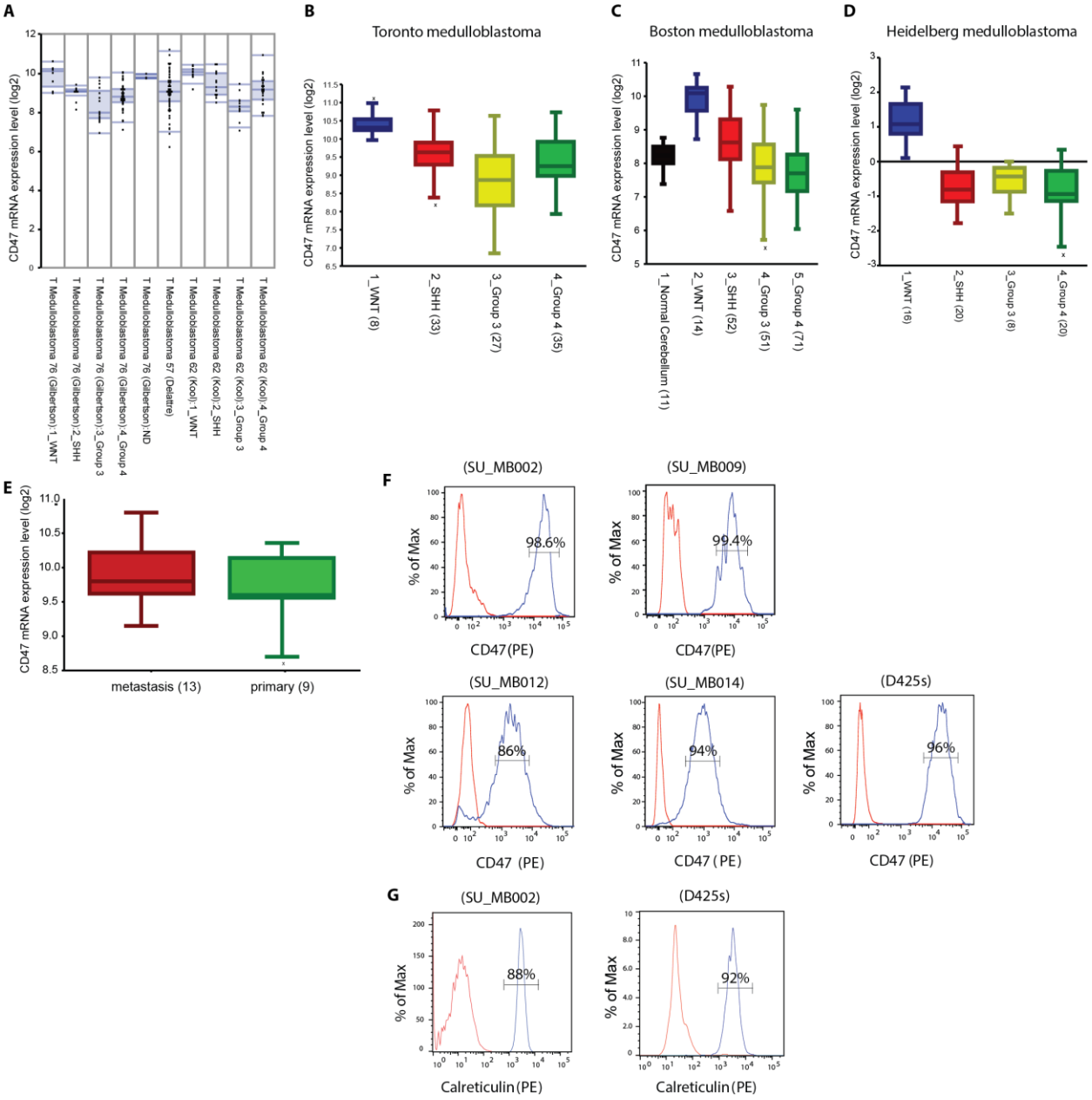

Fig. S1. Expression analysis of CD47 and cell surface CRT in MB. (**A**) Expression analysis of CD47 from the R2 dataset. Y-axis label is Log2 expression and expression values are depicted as

Box-Dot-Plot. Box plot component: In this plot type, the middle 50 percent of the data is represented by a box. The median forms a horizontal line within this box. The whiskers of this plot represent the extremes within the group. Dot plot component: Illustrates expression values observed in individual tumor samples. Expression analysis of CD47 across (**B**) Toronto, (**C**) Boston, and (**D**) Heidelberg datasets shows subgroup-specific expression of CD47. (**E**) Analysis of CD47 expression across medulloblastoma samples in primary site and metastatic regions. (**F**) Cell surface expression of CD47 on low passage (<10) primary patient-derived medulloblastoma cell lines as analyzed by flow cytometry. Flow cytometry analysis of CRT on SU_MB002 and D425s cells (**G**).

Supplementary Figure 2

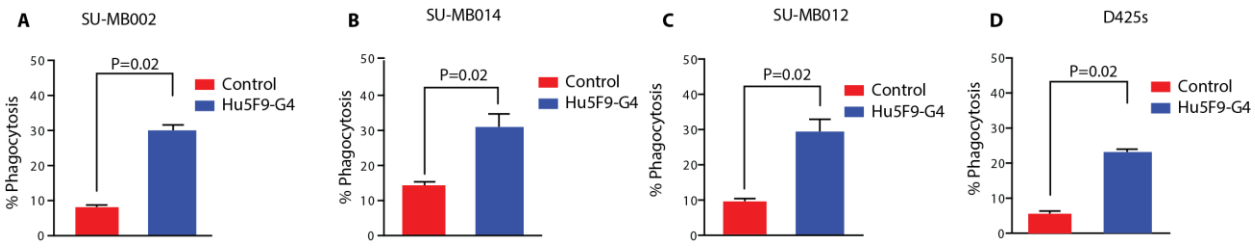

Fig. S2. Induction of potent macrophage-mediated phagocytosis of MB cells derived from surgical specimens by Hu5F9-G4. Phagocytosis assay was carried out as described in the Materials and Methods. Calcein AM-labeled tumor cells and macrophages were co-incubated in the presence of Hu5F9-G4 or IgG control. After an incubation period, cells were stained with anti-CD14 and anti-CD11b antibodies and analyzed on a flow cytometer. Macrophages were distinguished from tumor cells as being $CD14^{+}CD11b^{+}$. Macrophages with engulfed tumor cells in them were identified as $CD14^{+}CD11b^{+}Calcein^{+}$. Efficiency of phagocytosis was calculated as the percentage of macrophages with engulfed tumor cells in them. Data are shown from (**A**) SU_MB002, (**B**) SU_MB014, (**C**) SU_MB012, and (**D**) D425s MB cells. Cells were subjected to phagocytosis by macrophages from at least two different blood donors.

Supplementary Figure 3

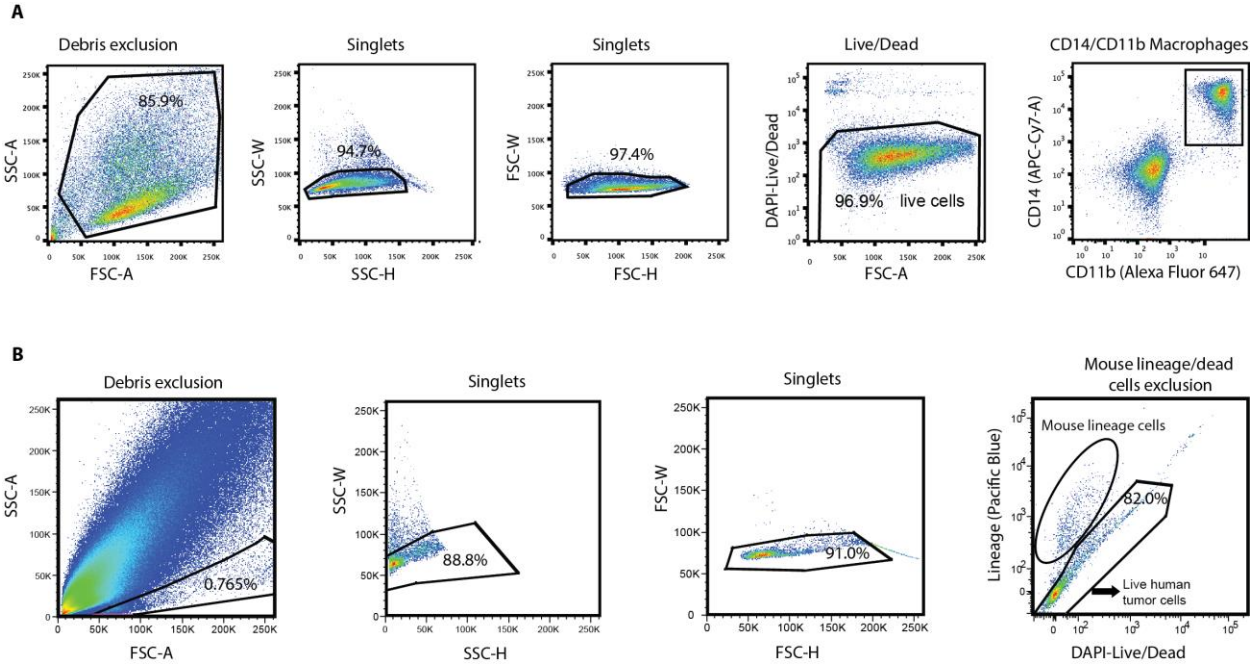

Fig. S3. Flow cytometry gating strategy. (**A**) Representative gating tree to illustrate the process used to select human macrophages for analysis of phagocytosis assay. Gating was done for debris exclusion (far left column), single cell isolation (left middle and middle column), and removal of dead cells (right middle column). Double positive CD14/CD11b cells were gated out to identify human blood-derived macrophages (far right column). (**B**) Representative sample gating of medulloblastoma xenografts from treated and control mice before brain tumor stem cell analyses. The tumors were dissociated and processed for removing debris (far left column), single cell isolation (left and right column), and purifying live population (far right column). The first SSC-A and FSC-A gate was re-drawn after back-gating for DAPI- (live)/mouse CD45-CD31-H2Kd- (mouse hematopoietic and endothelial lineage cells)/GFP+ (human cells).

Supplementary Figure 4

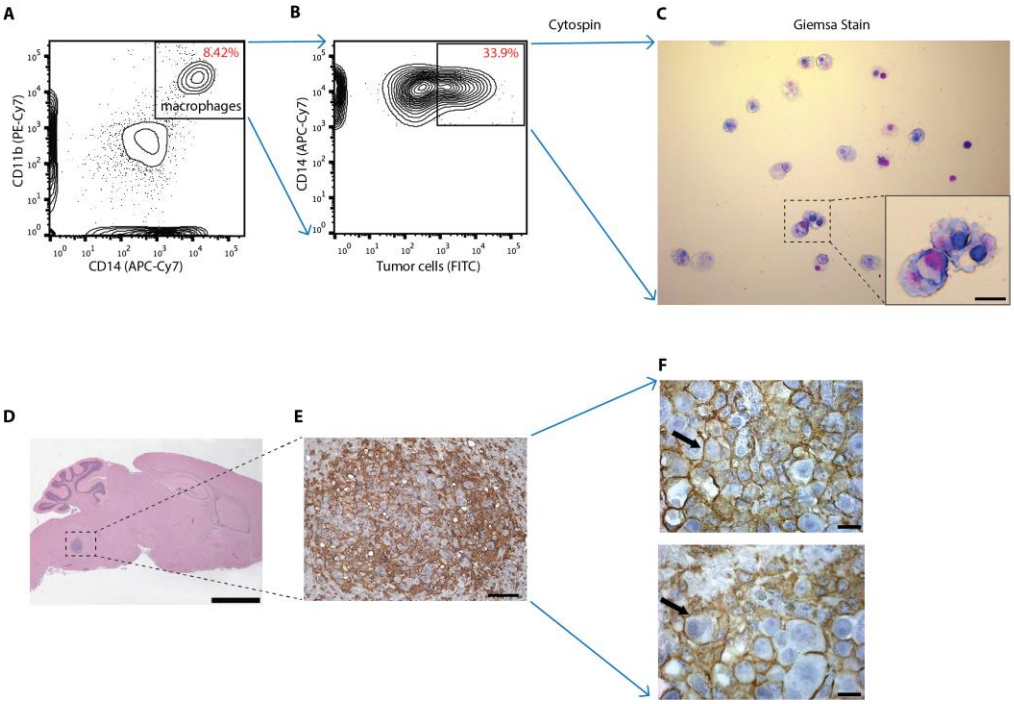

Fig. S4. Verification of phagocytic activity. (**A**) Macrophages were identified by their expression of CD14 and CD11b as detected by anti-CD14 and anti-CD11b antibodies, and the tumor cells were loaded with Calcein AM. (**B**) The populations of cells that was positive for macrophage markers and Calcein (FITC) were sorted out. (**C**) Wright-Giemsa stain on the sorted cells revealed the engulfment of MB cells by macrophages (scale bar, 50 μm). (**D**) H&E staining of SU_MB002 xenograft orthotopic tissue treated with Hu5F9-G4 (scale bar, 2 mm). (**E**) IHC staining for F4/80 protein (a mouse macrophage marker) revealed degraded medulloblastoma cells engulfed by macrophages (scale bar, 100 μm). (**F**) Higher magnification of (E) (scale bar, 200 μm).

Supplementary Figure 5

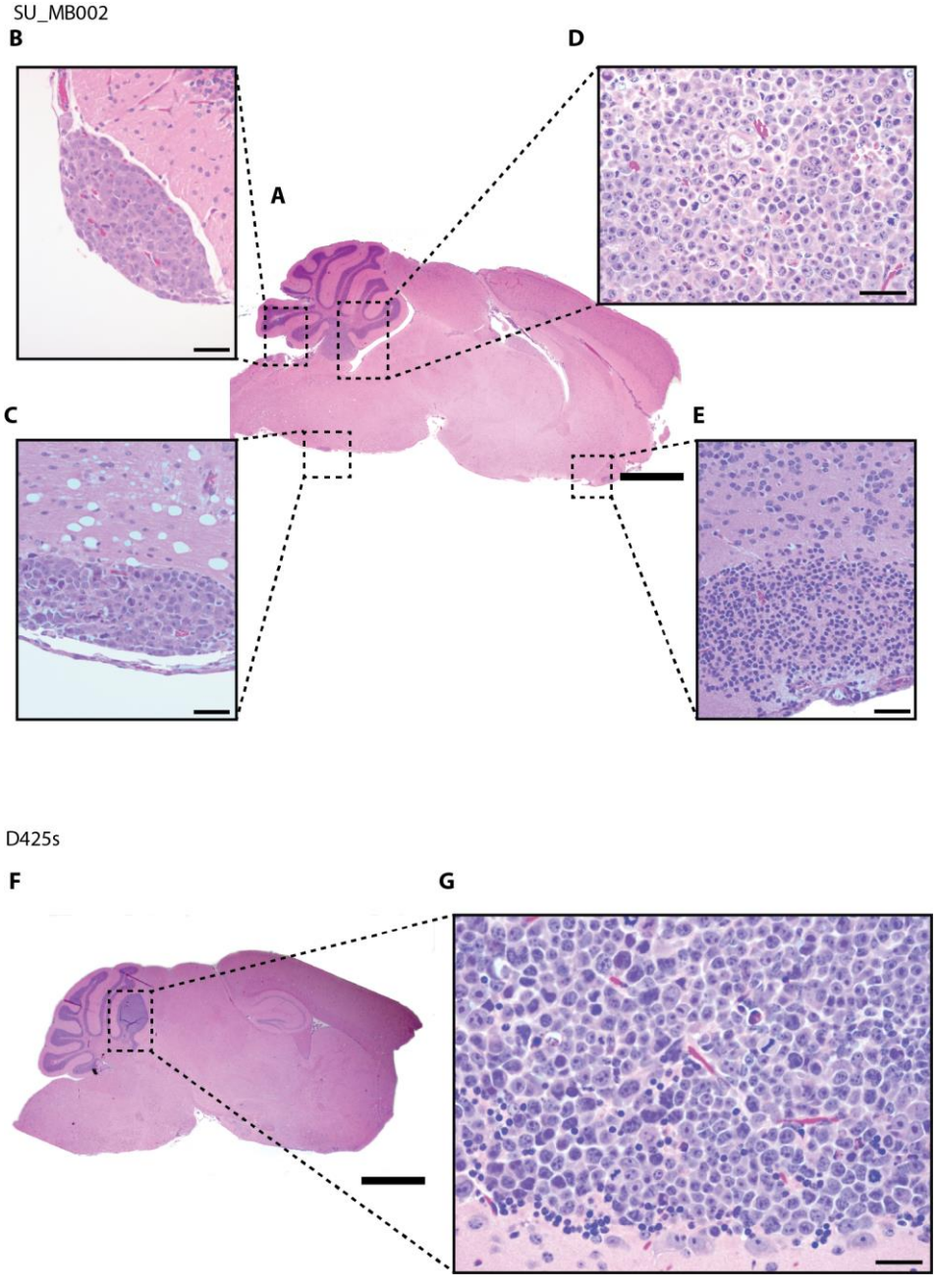

Fig. S5. Representative tumor burden at treatment initiation. H&E staining of SU_MB002 xenografts at the time of treatment initiation. (**A**) Cerebellar tumor seen in SU_MB002 xenograft shows leptomeningeal metastasis as well as intraventricular spread 5 d after tumor transplantation (scale bar, 2 mm). Higher magnification of tumor spread in (**B**) cerebellar pia, (**C**) pial bars of ventral pons, (**D**) IVth ventricle, and (**E**) inferior forebrain (scale bar, 100 μm). (**F**) H&E staining of D425s xenograft, d 5 after transplantation (scale bar, 2 mm). (**G)** Higher magnification of (F) (scale bar, 100 μm).

Supplementary Figure 6

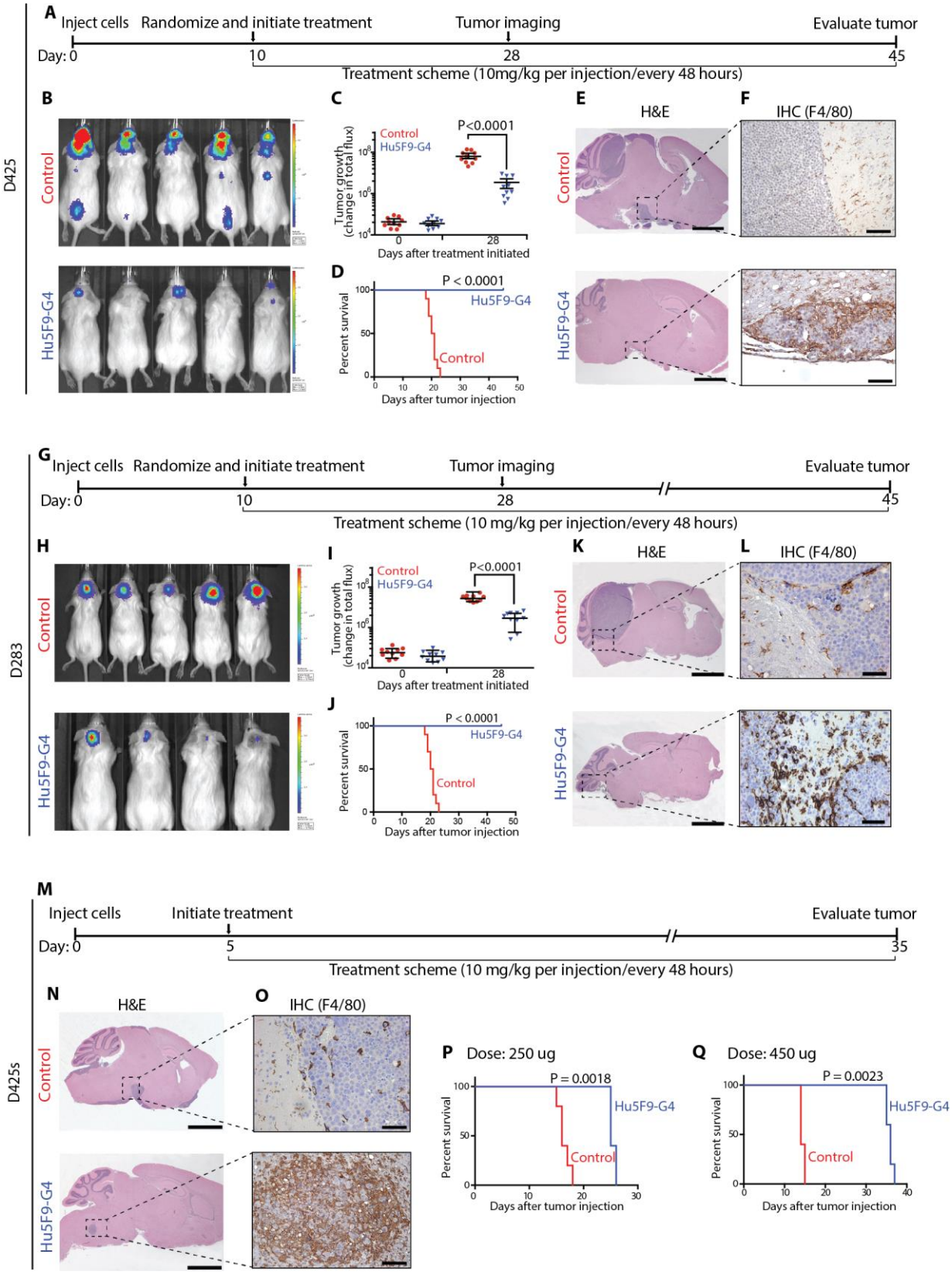

Fig. S6. Efficacy and dose-dependent response of Hu5F9-G4 in cell line–derived *cMYC*-amplified MB xenografts. (**A, G,** and **M**) Schematic timelines for study design. (**B, H**) Bioluminescence imaging from mice orthotopically injected with luciferase-expressing D425 and D283 lines, randomized and treated with Hu5F9-G4 or control. (**C, I**) Bioluminescence signal declined in Hu5F9-G4-treated versus control groups. (**D, J**) Significant improvement in survival is seen in Hu5F9-G4-treated mice compared to control group (**D**; D425, n= 10 per group, $P<0.0001$, log-rank analysis and **J**; D283, n= 10 per group, $P<0.0001$, log-rank analysis). (**E**, **K**) Representative H&E staining of brains from treated and control mice. Local and leptomeningeal tumor spread in control brain (**upper panel**) versus minimal tumor residue observed in treated brain (**lower panel**) (scale bars, 2 mm). (**F, L**) Immunohistochemistry staining of macrophages using the marker F4/80 shows increased macrophage infiltration in treated compared with control groups (scale bars, 50 μm). (**M-Q**) D425s, a subclone of D425 cell line, generated aggressive behavior with 100% penetrance of spontaneous spinal metastasis and high morbidity and mortality in xenograft setting. (**N**) H&E staining shows tumor burden in control brains compared with treated brains (scale bars, 2 mm). (**O**) IHC staining indicates macrophage involvement in tumor tissues in treated brains with Hu-5F9G4 compared with controls (scale bars, 50 μm). (**P, Q**) An increase in survival was achieved with Hu5F9-G4 treatment at a higher dose of 450 μg per mouse three times a week (**Q**, n= 5 per group, $P<0.0023$, log-rank analysis) compared to the standard dosing scale of 250 μg (**P**, n= 5 per group, $P<0.0018$, log-rank analysis).

Supplementary Figure 7

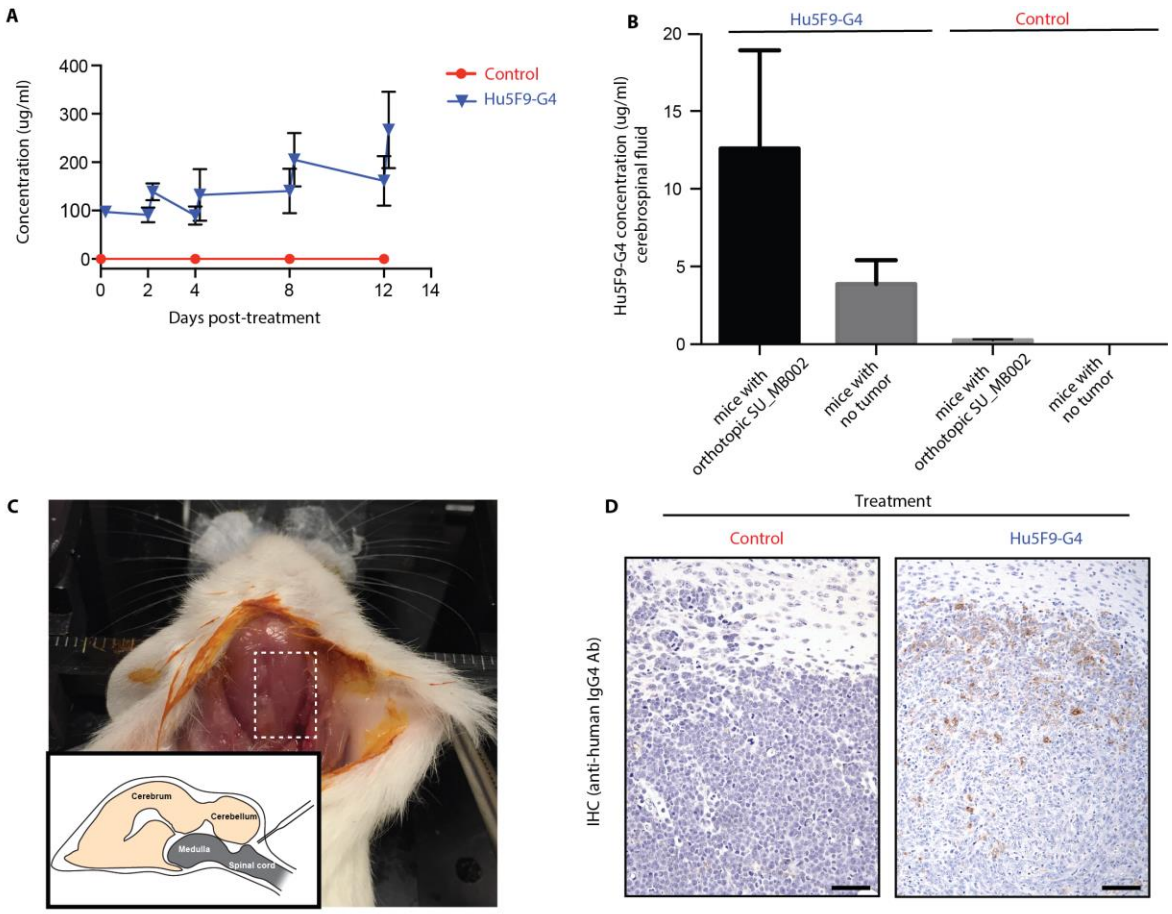

Fig. S7. Pharmacokinetic analysis and brain penetrance of Hu5F9-G4.

(**A**) Serum concentrations of Hu5F9-G4 in mice engrafted with SU_MB002 and treated every 48 h for 2 weeks with Hu5F9-G4 (100 μg/dose) were determined by ELISA. Serum was collected before treatment and 2 h after treatment with Hu5F9-G4 after the 1st, 2nd, 3rd, and 5th doses. (**B**) CSF was collected from mice orthotopically xenografted with MB tumor and mice without tumor. The mice were treated with Hu5F9-G4 for 2 weeks before CSF collection. CSF concentrations of Hu5F9-G4 were determined with ELISA test. The concentrations were

compared with the relevant values in control mice. (**C**) The image and sagittal schematic of a mouse brain with clear delineation of the spot for CSF collection. (**D**) IHC staining with anti-IgG4 antibody showed IgG4 staining in tissues treated with Hu5F9-G4 compared to control group (scale bars, 50 μm).

Supplementary Figure 8

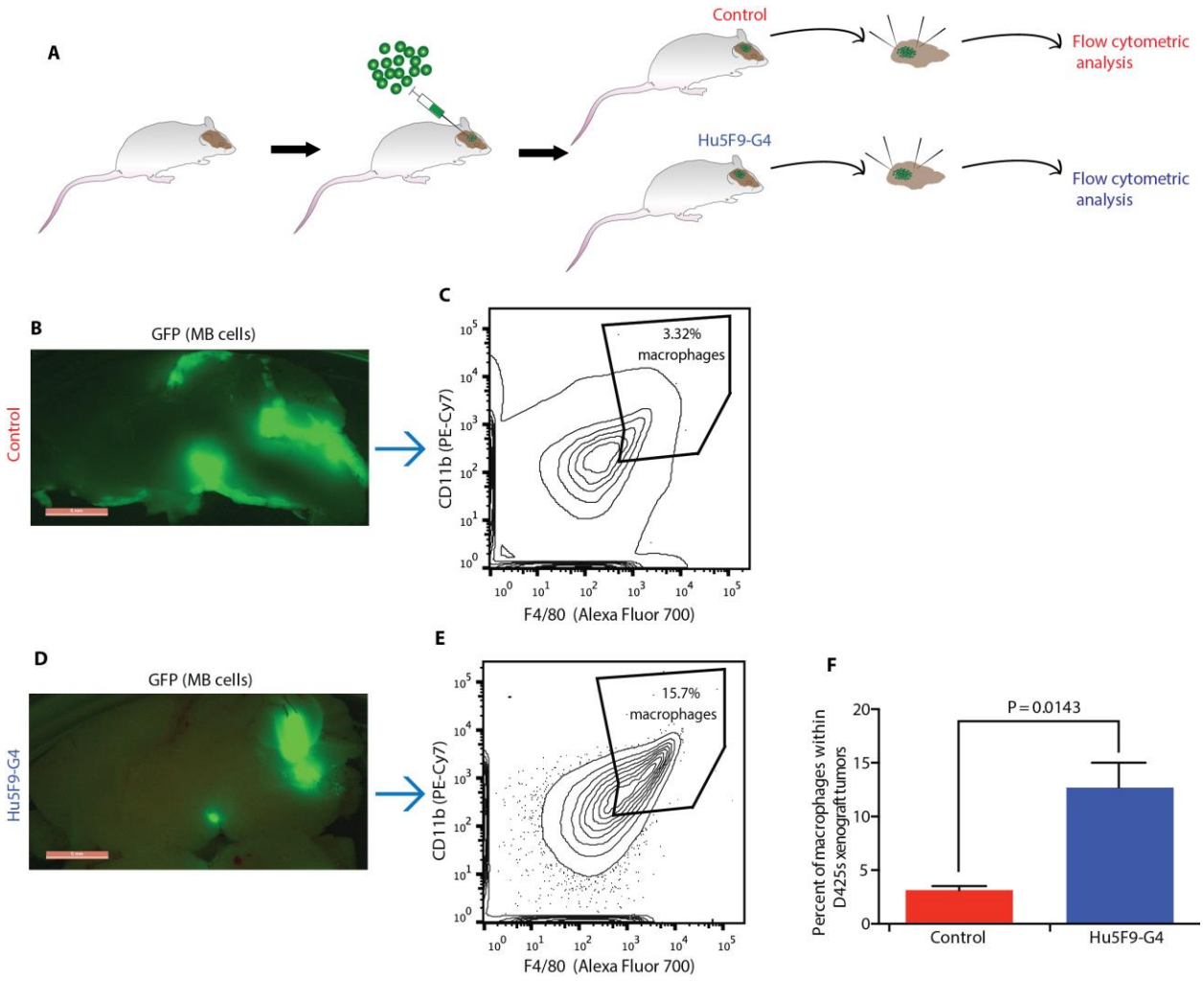

Fig. S8. Flow cytometric analysis of myeloid cell infiltration after Hu5F9-G4 treatment. (**A**) Schematic illustration of experimental design. (**B-F**) MB xenografts were treated with either control or Hu5F9G4 for 10 d, and the macrophage population in the tumor area was quantitated by flow cytometry. GFP and luciferase-expressing MB cells were orthotopically implanted in NSG mice. After 10 d of treatment with either control or Hu5F9-G4, the brains were dissected and a sagittal midline section was made. The sagittal sections were visualized under a fluorescent stereomicroscope. GFP fluorescence revealed large primary tumors and leptomeningeal tumor spread in the control brain (**B**), whereas only localized tumor was observed at the primary

cerebellar site with minimal residual leptomeningeal disease in the brain treated with Hu5F9-G4 (scale bars, 5 mm) (**D**). The GFP-expressing tumors were microdissected and dissociated for flow cytometric analysis. GFP^+ tumor cells were gated out. Within the GFP^- (mouse) cells, a significant (P=0.0143) increase in macrophage ($CD14^+$ and $CD11b^+$) was seen in Hu5F9-G4-treated brains (**E**) compared with the control groups (**C**). The percentage of recruited macrophages from three brains treated with Hu5F9-G4 compared with three brains from the control cohort (**F**).

Supplementary Figure 9

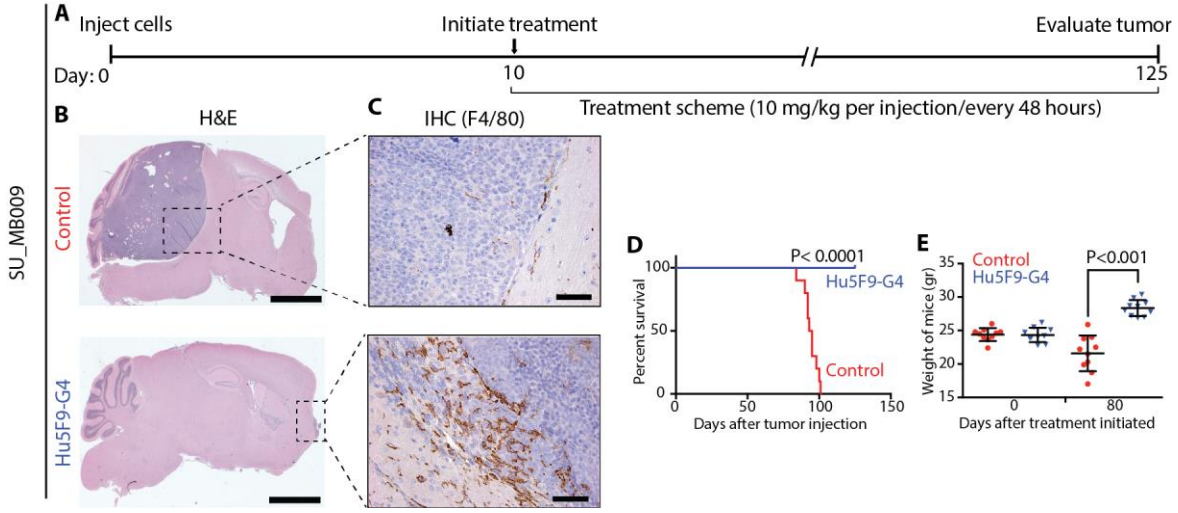

Fig. S9. Efficacy of Hu5F9-G4 against a primary patient-derived MB xenograft. (**A**) Treatment schema for the study design. (**B**) H&E staining shows tumor burden in control brains with SU_MB009 tumors compared with treated ones (scale bars, 2 mm). (**C**) IHC staining shows F4/80 positive macrophages in treated brain with Hu5F9-G4 (scale bars, 50 μm). (**D**) Significantly improved survival was seen in SU_MB009-bearing mice treated with Hu5F9-G4 (control=10, Hu5F9-G4=9, $P<0.0001$, log-rank analysis). (**E**) Mice xenografted with SU_MB009 and treated with Hu5F9-G4 had significantly higher weight compared with control mice 80 d after initiation of treatment ($P<0.001$).

Supplementary Figure 10

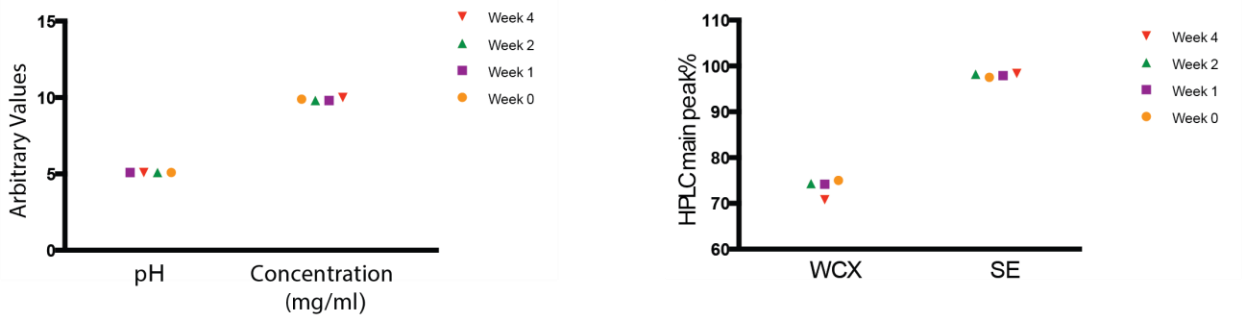

	Visual	pH	Concentration (mg/ml)	HPLC Main peak%	
				WCX	SE
T=0	Clear	5.1	9.9	75.0	97.5
T=1 week	Clear	5.1	9.8	74.2	97.9
T=2 week	Clear	5.1	9.8	74.3	98.2
T=4 week	Clear	5.1	10.0	70.8	98.4
T=8 week	Clear	5.3	10.1	65.9	98.1

Fig. S10. Stability of Hu5F9-G4. The stability of Hu5F9-G4 was studied by visual inspection, pH measurement, osmolality measurement, absorbance spectrophotometry, SDS-PAGE gel, weak cation exchange HPLC (WCX-HPLC), and size-exclusion HPLC (SE-HPLC). Hu5F9-G4 was stable for at least 2 months when stored at -70°C, 2-8°C and ambient temperature.

Supplementary Figure 11

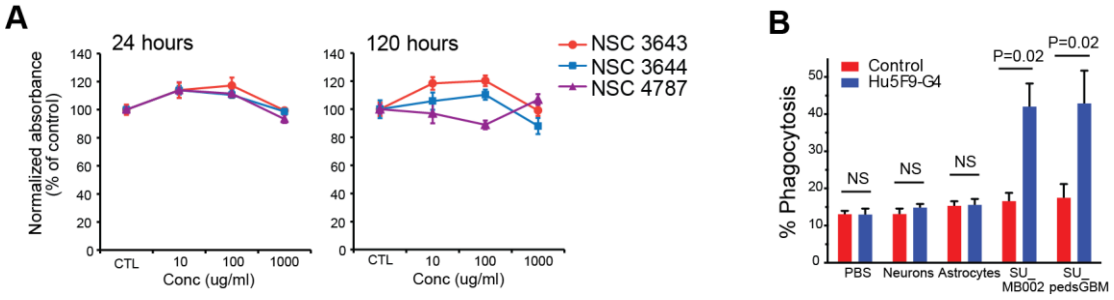

Fig. S11. Evaluating the toxicity of Hu5F9-G4 against human normal neural cells. (**A**) WST-1 assay for evaluation of neural progenitor cell viability after Hu5F9-G4 treatment at different concentrations after 24 h (left panel) and 120 h (right panel). Each colored line represents a different neural progenitor cell line derived from a different fetal specimen. (**B**) Phagocytosis of differentiated neural cells (neurons and astrocytes) and medulloblastoma cells co-cultured with macrophages and treated with either Hu5F9-G4 or PBS. No significant change was observed in phagocytosis of neurons and astrocytes treated with Hu5F9-G4 compared with their control counterparts, whereas medulloblastoma ($P<0.001$) and pGBM ($P<0.001$) cells treated with Hu5F9-G4 show significant engulfment by macrophages in the same experiment.

Supplementary Figure 12

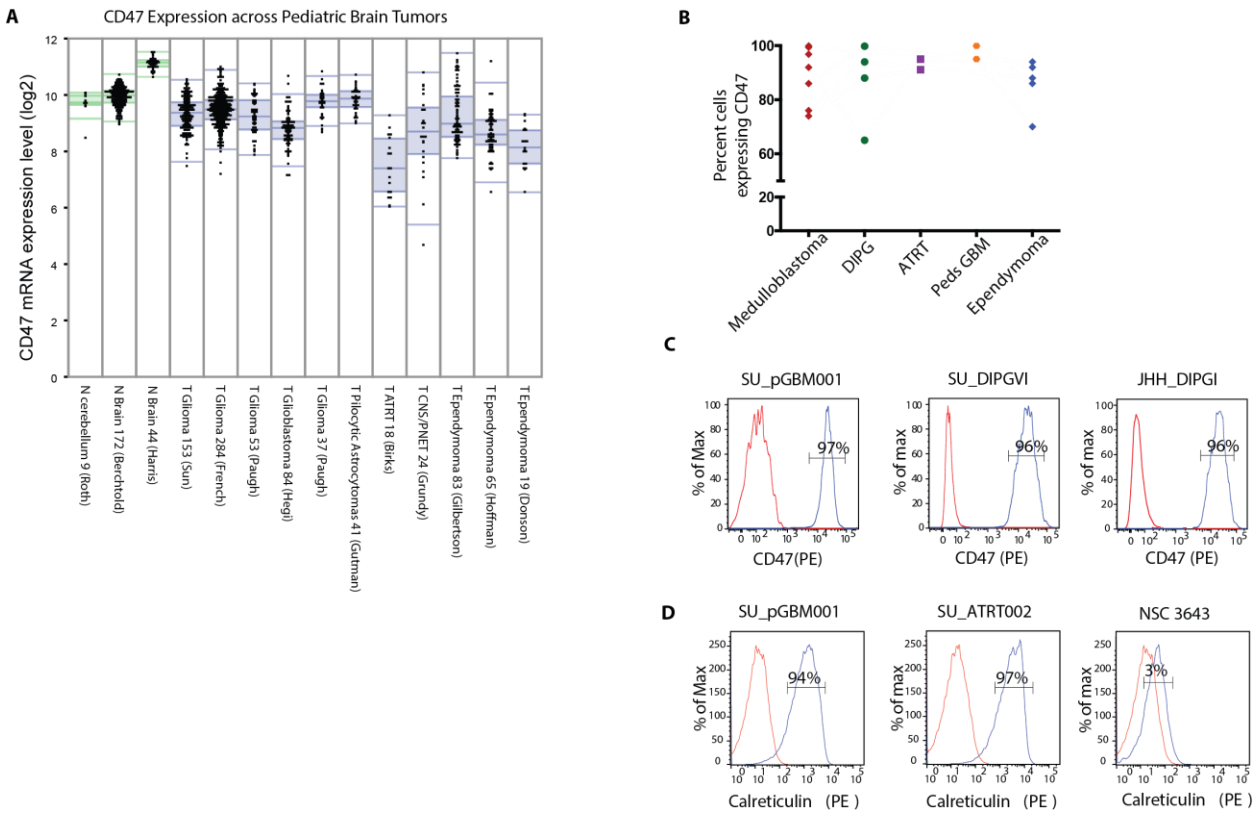

Fig. S12. CD47 and CRT expression on primary pediatric brain tumor samples. (**A**) CD47 expression across multiple databases for pediatric glioma, glioblastoma, pilocytic astrocytoma, ATRT, PNET, and ependymoma. Ubiquitous expression of CD47 is seen in all tumors analyzed. There is no significant difference in CD47 expression in tumors compared with normal brain or cerebellum. (**B**) Flow cytometric analysis of primary patient samples for surface expression of CD47. In most samples analyzed, >80% of the cells expressed CD47 on their surface. (**C**) Cell surface expression of CD47 in pediatric GBM and DIPG cancer stem cell lines. (**D**) Cell surface expression of CRT on patient-derived pediatric glioma, ATRT, and normal neural cell lines analyzed by flow cytometry.

Supplementary Figure 13

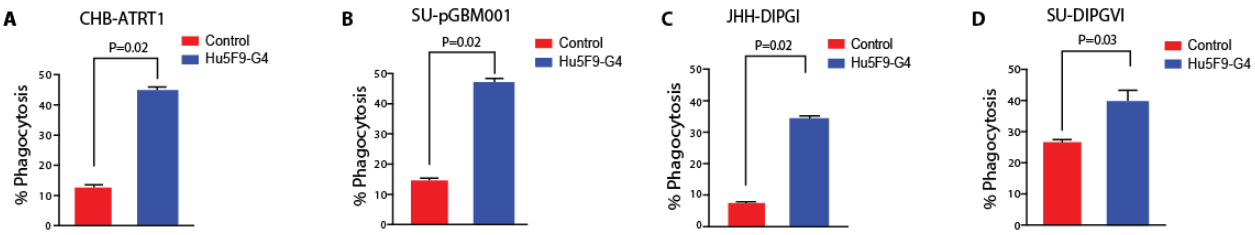

Fig. S13. Macrophage-mediated phagocytosis of pediatric brain tumor cells. Cells from three different pediatric brain tumor types, (**A**) CHB-ATRT1, (**B**) SU_pGBM001, (**C**) JHH-DIPGI, and (**D**) SU_DIPGVI, were labeled with Calcein AM and incubated with human peripheral blood-derived macrophages in the presence of 10 μg/nl Hu5F9-G4 or human IgG. Two hours later, the mixed samples were analyzed by flow cytometry to determine the percentage of phagocytosis. *P*-value was determined using a two-sided t-test.

Supplementary Figure 14

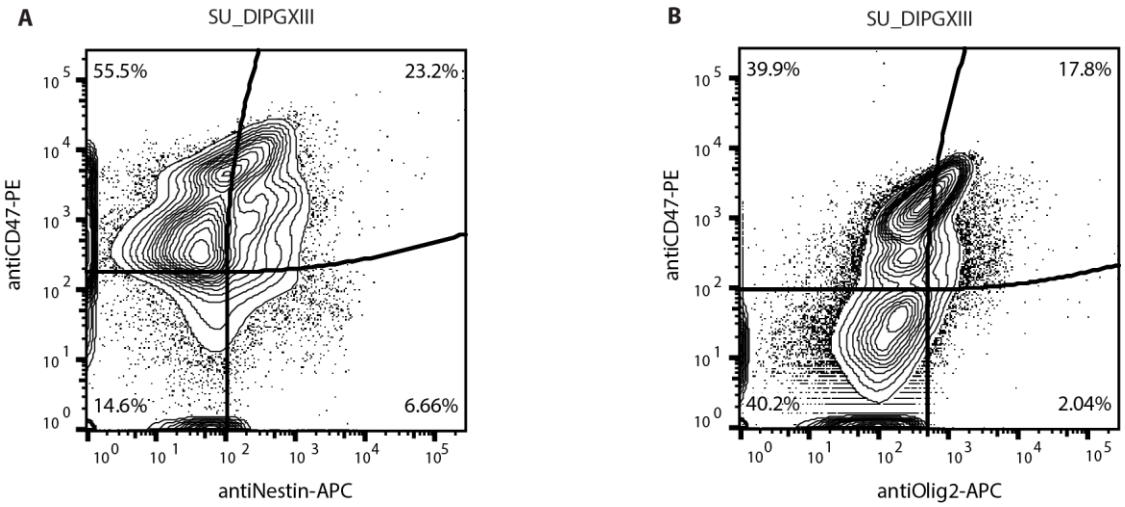

Fig. S14. High expression of Olig2 and Nestin on CD47^{+} DIPG cells. (A) CD47-positive cells with high expression of nestin. (**B**) Some CD47-positive cells expressed olig2

Supplementary Figure 15

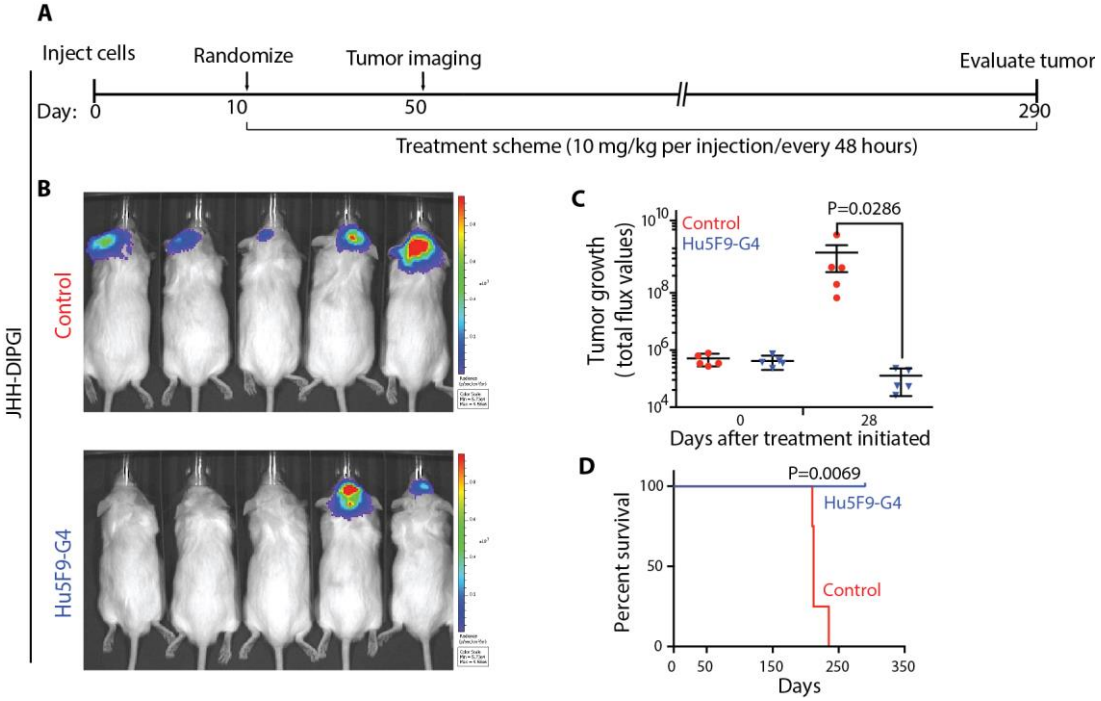

Fig. S15. Efficacy of Hu5F9-G4 in JHH-DIPGI xenografts. (**A-D**) In vivo anti-tumor efficacy of Hu5F9-G4 against JHH-DIPGI xenografts. Luciferase-expressing tumor cells were injected in the fourth ventricle (**B**) and treatment commenced after tumor was detected by bioluminescence imaging. (**C**) Significant decrease in total flux was observed after 34 weeks of treatment (p=0.0286). (**D**) Significant increase in survival was observed after Hu5F9-G4 treatment (p=0.006).

Supplementary Figure 16

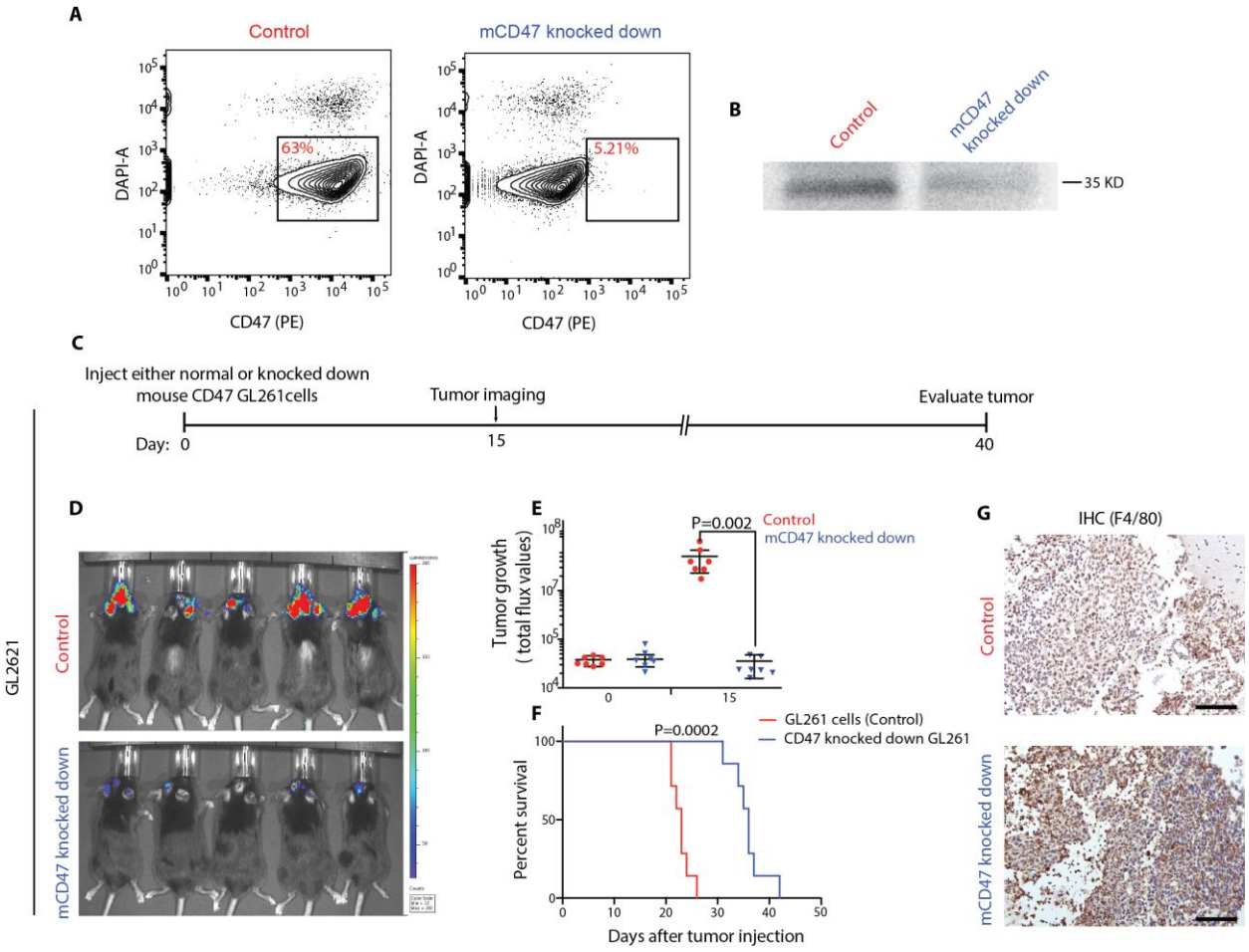

Fig. S16. Contribution of CD47 expression to tumor growth and phagocytosis by macrophages in an immunocompetent setting. (**A-F**) shRNA-dependent CD47 knockdown in GL261 cells slows down tumor growth in vivo. Analysis of cell surface expression of CD47 in control and CD47 knocked down GL261 by flow cytometry (**A**). Western blot analysis for total CD47 protein in GL261:CD47-KD cells and control. (**B**) Study design timeline (**C**) for mice orthotopically injected with either vehicle or CD47 knocked-down cells, and follow up BLI 15 days after tumor injection (shown in **D** and quantified in **E**). Significant extension in survival is seen in mice engrafted with CD47 knocked-down GL261 cell compared to control group (n= 7 per group, *P*=0.0002, log-rank analysis) (**F**). Immunohistochemical staining with F4/80 antibody

showed a notable macrophage presence in tumor tissues from knocked-down CD47 GL261 cells compared to control group (**G**).

Table S1. Quantitative IHC assessment of macrophage infiltration in vivo.

Tumor xenograft	Qualitative assessment of F4/80 staining (scale of 1 to 5)		Percent nuclei (eosin stain) surrounded by F4/80+ cytofilaments at tumor site	
	Hu5F9-G4	Control	Hu5F9-G4	Control
SU_pGBM002	3	1	80 %	9 %
SU_ATRT002	5	0	90 %	10 %
sPNET	5	0	90 %	8 %
SU_MB002	5	1	80 %	11 %
SU_MB009	4	1	50 %	10 %
D283	4	0	70 %	5 %
D425	4	0	60 %	10 %
D425s	5	1	80 %	9 %
GL261	4	1	60 %	20 %

Table S2. General characteristics of cell lines used in the study.

Cell line	Age at diagnosis (years)	Gender	Primary resection/ Post therapy	Site of resection	Known mutations/ Subgroups	Number of injected cells in vivo
SU_pGBM001						80,000
SU_pGBM002	12	Male	Primary resection		p53, EGFR amplification	80,000
SU_DIPGVI	7	Female	Post Therapy		H3.3 K27M	
SU_DIPGXIII	6	Female	Post Therapy		H3.3 K27M	100,000
JHH-DIPG-1			Obtained at autopsy			100,000
CHB-ATRT1	1	Female	Primary resection	Posterior-fossa		150,000
SU_ATRT002	2	Male	Primary resection	Supratentorial		150,000
sPNET	9	Female	Primary resection			80,000
SU_MB002	3	Male	Obtained at autopsy	Leptomeningeal spread	Group 3	30,000
SU_MB009	9	Female	Primary resection		Group 4	80,000
SU_MB012	6	Male	Primary resection	Primary site	Group 3	
SU_MB014					Group 3	
D283	6	Male	Primary resection	Metastatic site: peritoneum	Group 3	30,000
D425	5	Male			Group 3	30,000
D425s	10	Male	Primary resection of recurred tumor post therapy		Group 3	30,000
GL261	Mouse glioma line					300,000

Movie legends:

Movie S1. Qualitative behavioral assessment of SU_MB002 tumor-bearing mice treated with Hu5F9-G4 compared to control. SU_MB002 cells were transplanted into the cerebellum of NSG mice. Tumor engraftment was verified by bioluminescence (BLI) imaging and treated for 20 days with either Hu5F9-G4 or control. Mice treated with Hu5F9-G4 (right cage) maintained weight had normal feeding behavior and showed normal exploratory behavior. Mice in control group (left cage) exhibited cachexia, hunched back and decreased activity.

Movie S2. Qualitative behavioral assessment of D425s tumor-bearing mice treated with Hu5F9-G4 compared to control. D425s cells were transplanted into the cerebellum of NSG mice. Tumor engraftment was verified by bioluminescence (BLI) imaging and treated for 20 days with either Hu5F9-G4 or control. Mice treated with Hu5F9-G4 (left cage) maintained weight, had normal feeding behavior and showed normal exploratory behavior, whereas mice in control group (right cage) exhibited cachexia, hunched back, diminished eating and decreased activity.